Probing Dark Energy Dynamics from Current and Future Cosmological Observations

Gong-Bo Zhao[1,2][*] and Xinmin Zhang[3,4][†]

[1] *Institute of Cosmology and Gravitation, Dennis Sciama Building,*
Burnaby Road, Portsmouth, PO1 3FX, United Kingdom
[2]*Department of Physics, Simon Fraser University, Burnaby, BC, V5A 1S6, Canada*
[3]*Theoretical Physics Division, Institute of High Energy Physics,*
Chinese Academy of Sciences, P.O.Box 918-4, Beijing 100049, P.R.China
[4]*Theoretical Physics Center for Science Facilities (TPCSF), Chinese Academy of Sciences, P.R.China*

We report the constraints on the dark energy equation-of-state $w(z)$ using the latest 'Constitution' SNe sample combined with the WMAP5 and SDSS data. Assuming a flat universe, and utilizing the localized principal component analysis and the model selection criteria, we find that the ΛCDM model is generally consistent with the current data, yet there exists weak hint of the possible dynamics of dark energy. In particular, a model predicting $w(z) < -1$ at $z \in [0.25, 0.5)$ and $w(z) > -1$ at $z \in [0.5, 0.75)$, which means that $w(z)$ crosses -1 in the range of $z \in [0.25, 0.75)$, is mildly favored at 95% confidence level. Given the best fit model for current data as a fiducial model, we make future forecast from the joint data sets of JDEM, Planck and LSST, and we find that the future surveys can reduce the error bars on the w bins by roughly a factor of 10 for a 5-w-bin model.

I. INTRODUCTION

The apparent acceleration of the universe discovered at the end of last century remains an enigma [1, 2], and much effort has been made to find consistent explanation. This includes the modification or even the 'reinvention' of the Einstein gravity on large scales [3–11], and also the addition of the exotic energy budget – *Dark Energy* (DE) term to the right hand side of the Einstein equation. The *Equation-of-State* (EoS) w of dark energy, defined as the ratio of pressure and energy density, is usually used to classify different DE models. For example, the w of the simplest DE candidate, the vacuum energy, is a constant of -1, while w is generally considered as a function of redshift z for models predicting dark energy dynamics such as quintessence [12], phantom [13], quintom [14] and so forth.

It is true that we are still ignorant about the nature of dark energy, yet the accumulating high precision observational data of *Supernova Type Ia* (SNe), *Cosmic Microwave Background* (CMB) and *Large Scale Structure* (LSS) make it possible to study dark energy phenomenologically, i.e., confronting the numerous dark energy models to data and narrowing down the dark energy candidates by falsifying part of the models, which might be the best we can do to approach the truth of dark energy. In this data-driven investigation, in most cases one needs to parameterize $w(z)$ in the first place, i.e. assume an *ad hoc* functional form of $w(z)$, then fit the related parameters to data, reconstruct $w(z)$ and make statements according to the result of the reconstruction [15]. Since the result may more or less depend on the assumed form of $w(z)$, and to minimize the artifacts, one needs to choose the parametrization with care – it should be physically moti-

vated, and statistically sound, i.e., using the least number of free parameters to obtain the maximum generality.

The first example of the viable parametrization is the widely used CPL parametrization [16, 17],

$$w(a) = w_0 + w_a \frac{z}{1+z} \qquad (1)$$

where w_0 and w_a are free parameters. It is widely used since it has a simple form, clear interpretation – w_0 is the EoS today and w_a denotes the derivative with respective to the scale factor a, thus a dark energy dynamics indicator – and a small number of free parameters. However, the simplicity of the form inhibits the CPL parametrization to describe the models whose EoS deviates significantly from the linear function of a, for example, a $w(z)$ with oscillations [18], or with other local features [19].

One alternative is to approximate $w(z)$ using the piecewise constant bins [20], which is much more general than the functional parametrizations. This generality allows for the high-resolution temporal reconstruction of $w(z)$, based on which one can make further model-independent studies using a *Principal Component Analysis* (PCA) method [20–27]. For example, it is possible to know how many EoS parameters can be well constrained by current/future data regardless of the forms of parametrization; where is (are) the sweet spot(s) (the redshift where the error on $w(z)$ gets minimized); and we can even construct the uncorrelated bands to probe dark energy dynamics more explicitly from the cosmological observations [21, 25, 28, 29] [1]. Given the constraints on $w(z)$ from the current data, it is useful to know to what extent the future surveys will tighten the constraints. In this paper, we will focus on the *Uncorrelated Band-power Estimates*

---

[*]Electronic address: Gong-bo.Zhao@port.ac.uk
[†]Electronic address: xmzhang@ihep.ac.cn

[1] Aside from PCA, other less model-dependent methods have been developed, such as smoothing the SN data to derive $w(z)$ [30], constraining the binned dark energy density [31], etc.

(UBE) of $w(z)$ from the current and the simulated future data.

In the next section, we will describe the method and data we use in detail and in section III we will present our main results, and then we will finish with the summary and discussion.

II. METHODOLOGY AND DATA

A. Constraining dark energy from current observations

To fit to data, we parametrize our universe as:

$$\mathbf{P} \equiv (\omega_b, \omega_c, \Theta_s, \tau, n_s, A_s, \mathcal{X}) \qquad (2)$$

where $\omega_b \equiv \Omega_b h^2$ and $\omega_c \equiv \Omega_c h^2$ are the physical baryon and cold dark matter densities relative to the critical density respectively, Θ_s stands for the ratio (multiplied by 100) of the sound horizon to the angular diameter distance at decoupling, τ denotes the optical depth to reionization, and n_s, A_s are the primordial power spectrum index and amplitude, respectively. We assume a flat universe throughout.

The dark energy EoS parameters are denoted by $\mathcal{X}$, and we consider the following two kinds of parametrizations in this work,

$$w(z) = \begin{cases} \text{Sum of the tanh bins,} & \mathcal{X}_{\mathrm{I}} = \{w_i\}; \\ w_0 + w_a \cdot z/(1+z), & \mathcal{X}_{\mathrm{II}} = \{w_0, w_a\}; \end{cases} \qquad (3)$$

where $\mathcal{X}_{\mathrm{I}}$ and $\mathcal{X}_{\mathrm{II}}$ are the collections of the bin parameters for dark energy equation of state (see explanations below) and the CPL parameters respectively, and the constraints on these parameters allow us to reconstruct the evolution history of $w(z)$, which might encode the dark energy dynamics.

For dark energy parametrization $\mathcal{X}_{\mathrm{I}}$, we approximate $w(z)$ using the sum of N piecewise constant bins w_i localizing in redshift and vary them to fit data. The simplest realization of this binning is to use step functions [20, 25, 28, 29]. However, the resulting discontinuity in $w(z)$ makes it difficult to handle dark energy perturbations, which depends on the time derivative of $w(z)$ and plays a crucial role in the parameter estimation, and should be treated in a consistent way [32–34]. To solve the problem of discontinuity, one can use the smooth and differentiable functions such as the cubic spline functions [21, 22], and the hyperbolic tangent functions [24] for the binning. Here we follow the latter and parameterize $w(z)$ as,

$$w(z) = \sum_{i=1}^{N-1} \frac{(w_{i+1} - w_i)}{2} \left[1 + \tanh\left(\frac{z - z_{i+1}}{\xi}\right) \right] + w_1 \qquad (4)$$

where w_i denotes the value of EoS in the ith bin, and z_i, z_{i+1} stand for the endpoints of the ith bin. Also note

that ξ is the transition width of two neighboring bins, and is set to 5% of the bin width. We have numerically checked that the final result is largely independent of ξ as long as it describes a sharp, but numerically stable transition. For a total of N-bin parametrization, we arrange the first $N - 1$ bins to be evenly spaced at low redshifts ($z \leq 1$), and use one wide bin to model $w(z)$ at $z > 1$ since dark energy becomes less and less important as redshift increases, and it has been found that there is no hope to resolve dark energy dynamics, if any, beyond redshift one even using the future *Joint Dark Energy Mission* (JDEM) survey [20, 35]. In our numerical analysis, we let all the N bins (including the high-z bin) float in all cases, thus our constraint on $w(z)$ at low-z is more conservative than that with fixed high-z bin. Note that in our notation, $N = 1$ corresponds to the wCDM model where w is a constant regardless of redshift, and $N = 0$ stands for ΛCDM model.

It is true that the larger N we use, the higher temporal resolution we can obtain. However, the result will be severely diluted for large N. This is not only due to the weakness of current data, but also to the huge degeneracy introduced. Therefore we need a criterion to determine the optimal number of bins, so that we can detect the main features from data by using the minimal number of bins. This is an issue of Occam's razor, i.e., we don't want to introduce unnecessary parameters. To optimize the *Goodness of Fit* (GoF), we search for an optimal N in the range $N \in [0, 10]$ based on the model selection criteria which we will describe in detail in Sec. III. Then $w(z)$ can be reconstructed from data.

However, the interpretation of the reconstructed $w(z)$ might be obscured by the correlations among the dark energy bins. To eliminate this ambiguity, one seeks for a linear transformation $\mathcal{W}$ to rotate the original parameter vector $\mathcal{X}$ into a new parameter vector $\mathcal{Q} = \mathcal{W}\mathcal{X}$ so that the resultant new parameters, denoted by the q's, are physically and statistically meaningful, namely, they directly relate to the w bins and have uncorrelated errors.

This is an eigenvalue/vector problem, and can be solved by applying the linear manipulations on the covariance matrix $\mathbf{C}$ of the w bins (after marginalizing over the other cosmological parameters):

$$\mathbf{C}_{\mathcal{X}_{\mathrm{I}}} = (w_i - \langle w_i \rangle)(w_j - \langle w_j \rangle)^T = \langle \mathcal{X}_{\mathrm{I}} \mathcal{X}_{\mathrm{I}}^T \rangle \qquad (5)$$

We then diagonalize the Fisher matrix $\mathbf{F} \equiv \mathbf{C}^{-1}$ so that $\mathbf{F} = \mathbf{O}^T \mathbf{\Lambda} \mathbf{O} = \mathcal{W}^T \mathcal{W}$. Here $\mathbf{O}$ is the orthogonal matrix, $\mathbf{\Lambda}$ is diagonal and $\mathcal{W} = \mathbf{F}^{1/2}$. Then the resulting transformation matrix $\mathcal{W}$, obtained by absorbing $\mathbf{\Lambda}^{1/2}$ into $\mathbf{O}$, can make the new parameters q's uncorrelated and the weights (rows of $\mathcal{W}$) are nearly positive definite and localized in redshift, which means that q_i has a one-to-one correspondence to w_i (and close to w_i), making the interpretation more transparent [21, 25, 28, 29]. To make $q(z) = -1$ stand for ΛCDM, we re-scale $\mathcal{W}$ so that its rows sum up to unity, i.e. $\mathcal{W}_{ij} = F_{ij}^{1/2}/(\sum_k F_{ik}^{1/2})$. Note, however, that the normalization is arbitrary and

the physical inferences do not depend on this normalization as both the parameters q's and their values for a particular theoretical model change consistently [21]. Before normalization, the variances of the q's are unity since

$$\mathbf{C}_{\mathcal{Q}} = \langle \mathcal{Q}\mathcal{Q}^T \rangle = \mathcal{W}\langle \mathcal{X}_{\mathrm{I}}\mathcal{X}_{\mathrm{I}}^T \rangle \mathcal{W}^T = \mathbf{F}^{1/2}\mathbf{C}\mathbf{F}^{1/2} = \mathbf{I} \quad (6)$$

While after normalization, the covariance matrix becomes $\langle \Delta q_i \Delta q_j \rangle = \delta_{ij}/(\sum_a F_{ia}^{1/2} \sum_b F_{jb}^{1/2})$. This prescription is called the Uncorrelated Band-power Estimate, or *Localized Principal Component Analysis* (LPCA).

Parametrization $\mathcal{X}_{\mathrm{II}}$ is a widely used functional form for dark energy EoS, but it needs to be tested whether this linear function of scale factor is general enough to describe dark energy for the current data. This can be done by reconstructing $w(z)$ from parametrizations $\mathcal{X}_{\mathrm{I}}$ and $\mathcal{X}_{\mathrm{II}}$ respectively, and then making a direct comparison.

Given the set of cosmological parameters $\mathbf{P}$ in Eq (2), we calculate the observables including the luminosity distance, CMB and matter power spectra, and the cosmic age using our modified version of CAMB[2], which is able to calculate all the necessary observables for an arbitrary $w(z)$. We pay particular attention to the Dark Energy Perturbations (DEP), especially when $w(z)$ crosses -1. Our calculation for DEP for general dark energy models is based on the work presented in Ref. [33]. We then fit to SNe, CMB and LSS observations using a modified version of the Markov Chain Monte Carlo (MCMC) package CosmoMC[3][36] based on the Bayesian statistics.

The supernova data we use are the recently released "Constitution" SALT sample [37], and we marginalize over the nuisance parameter, which is basically the calibration uncertainty in measuring the supernova intrinsic magnitude, in the likelihood calculation. For CMB, we use the WMAP five-year data including the temperature and polarization power spectra [38], and calculate the likelihood using the routine supplied by the WMAP team[4]. For the LSS information, we use the Sloan Digital Sky Survey (SDSS) Luminous Red Galaxy (LRG) sample [39], and marginalize over the bias parameter. Furthermore, we impose the $1 - \sigma$ Gaussian priors on the Hubble parameter and baryon density of $h = 0.72 \pm 0.08$ and $\Omega_b h^2 = 0.022 \pm 0.002$ from the measurements of Hubble Space Telescope (HST) [40] and Big Bang Nucleosynthesis [41] respectively, and a tophat prior on the cosmic age of 10 Gyr $< t_0 <$ 20 Gyr. The total likelihood is taken to be the products of the separate likelihoods $\mathcal{L}$ of each dataset we used, thus the total χ^2 is the sum of separate χ^2 from individual observations plus that from the priors if we define $\chi^2 \equiv -2\log\mathcal{L}$.

B. Future Forecast

Given the current constraints on dark energy, it is useful to know quantitively how future surveys can improve the constraints. Therefore we choose the best fit $w(z)$ from current data as a fiducial model, and make a forecast from the surveys of JDEM, Planck [42] and *Large Synoptic Survey Telescope* (LSST) [43] by employing a standard Fisher Matrix technique following [44].

1. Observables and Fisher Matrices

Besides the luminosity distance and the CMB power spectra simulated for JDEM and Planck respectively, we include the tomographic observables including the spectra of the *Galaxy Counts*(GC) and *Weak Lensing*(WL) from LSST, and all the possible cross-correlations with CMB. Mathematically, all the tomographic observables we use can be summarized as

$$C_\ell^{XY} = 4\pi \int \frac{dk}{k} \Delta_{\mathcal{R}}^2 I_\ell^X(k) I_\ell^Y(k), \quad (7)$$

where $\Delta_{\mathcal{R}}^2$ is the primordial curvature power spectrum and $I_\ell^{X,Y}(k)$ denotes the angular transfer functions. Here $X, Y \in [T, E, G_i, \epsilon_j]$, where T, E, G_i and ϵ_j illustrate the CMB temperature, E-mode polarization, the ith redshift bin for galaxy counts and the jth redshift bin for weak lensing shear respectively. In other words, we consider all the possible cross-correlations among CMB, GC and WL.

Given the specifications of the proposed future surveys, the tool of Fisher matrix [45] enables us to quickly estimate the errors on the cosmological parameters around the fiducial values. For zero-mean Gaussian-distributed observables, such as C_ℓ^{XY}, the Fisher matrix is given by

$$F_{\alpha\beta} = f_{\mathrm{sky}} \sum_{\ell=\ell_{\min}}^{\ell_{\max}} \frac{2\ell+1}{2} \mathrm{Tr}\left(\frac{\partial \mathbf{C}_\ell}{\partial p_\alpha}\tilde{\mathbf{C}}_\ell^{-1}\frac{\partial \mathbf{C}_\ell}{\partial p_\beta}\tilde{\mathbf{C}}_\ell^{-1}\right), \quad (8)$$

where $p_{\alpha(\beta)}$ is the $\alpha(\beta)$th cosmological parameter and $\tilde{\mathbf{C}}_\ell$ is the "observed" covariance matrix with elements $\tilde{C}_\ell^{XY}$ that include contributions from noise:

$$\tilde{C}_\ell^{XY} = C_\ell^{XY} + N_\ell^{XY}. \quad (9)$$

The expression (8) assumes that all fields $X(\hat{\mathbf{n}})$ are measured over contiguous regions covering a fraction f_{sky} of the sky. The value of the lowest multipole can be estimated from $\ell_{\min} \approx [\pi/(2f_{\mathrm{sky}})]$, where the square brackets denote the rounded integer.

In general, the noise matrix N_ℓ^{XY} receives the contributions from both the statistical and the systematic errors. For the statistical error, we assume the uncorrelated Poisson noise on the galaxy overdensity in each galaxy bin (G_i) and shear fields (ϵ_i), the noise is given
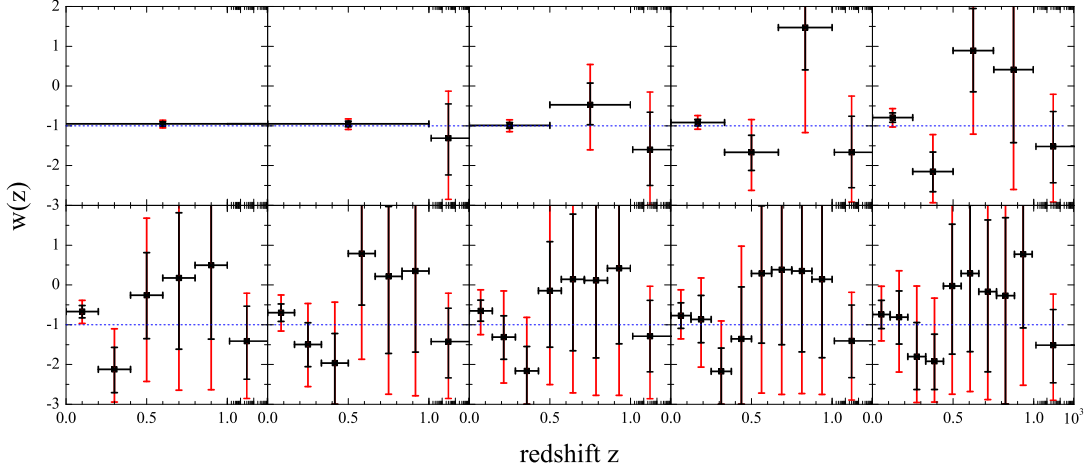
FIG. 1: The correlated binned estimates of the EoS from current observational data. The black and red error bars show 1σ and 2σ uncertainties respectively. The blue dashed line shows ΛCDM model.
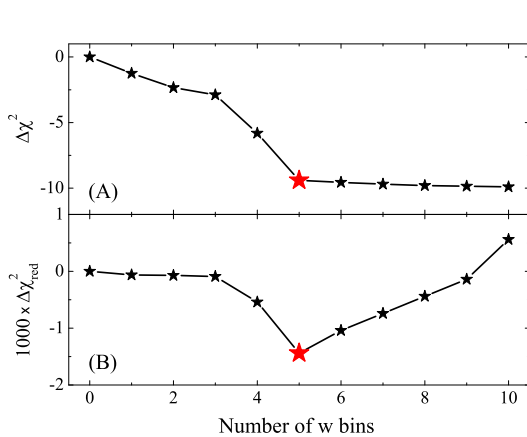

FIG. 2: The improved χ^2 and reduced χ^2 w.r.t. the ΛCDM model as a function of the number of w bins. The big red stars illustrate the optimal model.
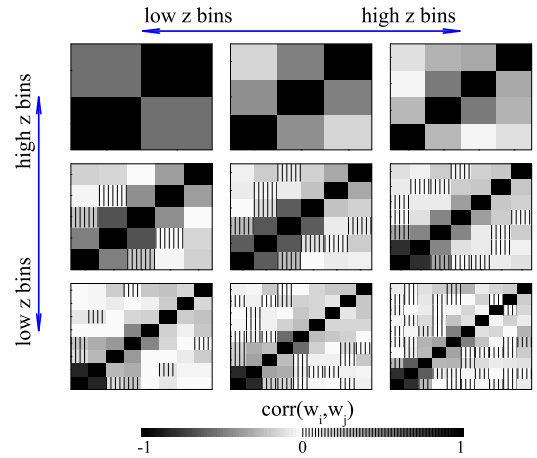

FIG. 3: The correlation matrices for the w bins for different binnings. From upper left to lower right, we show the correlation matrices for $N = 2$ to $N = 10$ binnings (high-z bin inclusive in all cases, as stated in the main text).

by [46]

$$N_\ell^{\epsilon_i \epsilon_j} = \delta_{ij} \frac{\gamma_{\rm rms}^2}{n_j}$$

$$N_\ell^{G_i G_j} = \delta_{ij} \frac{1}{n_j}$$

$$N_\ell^{G_i \epsilon_j} = 0, \qquad (10)$$

where $\gamma_{\rm rms}$ is the expected root mean square shear of the galaxies, and n_j is the number of galaxies per steradian in the jth redshift bin.

Besides the shot noise, we follow [47] and consider three classes of the systematics: redshift errors, addi-

tive errors and multiplicative errors [5]. The redshift errors may stem from three sources: the distortion of the total galaxy distribution, z-bias and z-scatter. In our calculation, we marginalized over 30 Chebyshev expansion coefficients describing the distortion to the overall shape of the galaxy distribution; one redshift bias parameter and one redshift scatter parameter for each redshift bin

---

[5] Systematics are notoriously difficult to model and predict for the forecast, and it can also stem from some physical processes such as the baryonic uncertainty studied in [48]. But we didn't include this effect for simplity.

to account for the uncertainty of the redshift measurement of the bins. The additive error can be generated by the anisotropy of the *Point Spread Function* (PSF) and they generally present for both galaxy counts and lensing shear bins. Following [47], we parametrize the additive error as

$$(C_\ell^{\mathrm{XY}})_{ij} = \delta_{\mathrm{XY}} \rho A_i^{\mathrm{X}} A_j^{\mathrm{Y}} \left(\frac{\ell}{\ell_*^{\mathrm{X}}}\right)^\eta \tag{11}$$

and choose $\rho = 1, \eta = 0$. The fiducial values of the A's are chosen to be conservative, $(A_i^{\mathrm{g}})^2 = 10^{-8}, (A_i^\gamma)^2 = 10^{-9}$. The multiplicative errors in measuring the shear can be parameterized as,

$$(\widetilde{C}_\ell^\gamma)_{ij} = (C_\ell^\gamma)_{ij}[1 + f_i + f_j]. \tag{12}$$

2. Experiments and Cosmological Parameters

As mentioned before, the data considered in our forecast include the SNe observations, CMB power spectra of temperature and polarization (T and E), WL, GC, and their cross-correlations. We assume CMB T and E data from the Planck satellite [42], the galaxy catalogues and WL data by the LSST [43], complemented by a futuristic SNe data set provided by a future JDEM space mission. We strictly follow [44] to set up the the survey parameters. In our forecasts, we use the best fit values of the cosmological parameters obtained from current data as a fiducial model, and impose a Gaussian prior on the value of h from the Hubble Space Telescope (HST) [40]. We assign a constant bias parameter for each galaxy bin, and then marginalize over.

III. RESULTS

Before viewing the results for parametrization $\mathcal{X}_{\mathrm{I}}$, one might be able to make an 'intuitive guess' based on the following reasoning. As elaborated in Sec. II, we attempt to 'see' the possible dark energy dynamics by placing numerous w bins around -1 to fit data. If the real dark energy EoS were -1, then the number of bins (and even the method of binning) shouldn't affect the fit much, i.e., the $\Delta\chi^2$ would have little dependence on the number of w bins[6]. However, if dark energy were dynamical, e.g., there exist some local features in $w(z)$ on some scale, the w bins wander around -1 trying to find a better fit to data than $w = -1$, and the $\Delta\chi^2$ behavior would be strongly depend upon the number of w bins. Consider, if the binning is coarse, then it might not be able to resolve the features

in $w(z)$ properly, and this might result in the marginal improvement on χ^2. However, if the binning resolution is fine enough allowing $w(z)$ to vary on the scale of main feature of $w(z)$, the bins may gain sufficient freedom to capture the principal features in the data set, giving rise to sharp drops on χ^2. It is true that using finer binning can in principle improve χ^2 further, but it is not effective to improve the reduced χ^2, which is an indicator of the goodness of fit, and is defined as,

$$\chi_{\mathrm{red}}^2 \equiv \chi^2/\nu \tag{13}$$

where ν denotes the number of degrees of freedom in the fit, i.e., the number of data points subtracted by the number of fit parameters defined in Eq. (2). For a reliable fit, the χ_{red}^2 should be close to unity, which is the case for all our 10 fits shown in Fig 1. For example, for our base model (ΛCDM), the χ^2 is 3149.06 for 2978 degrees of freedom, giving $\chi_{\mathrm{red}}^2 = 1.057$.

Using a unnecessary large number of bins can hardly improve the fit. On the one hand, the super fine bins can do nothing more but resolve the unimportant feature in the data, or overfit the data by treating the noise as features, so that they cannot improve the χ^2 drastically. On the other hand, the redundant bins will be highly correlated, making it difficult to extract useful information from data by performing the global fit even if the MCMC algorithm is used. Therefore, there is a trade-off between the number of w bins N and the GoF, and it is a necessity to seek for the optimal N maximizing the GoF.

Now let's look at the reconstructed $w(z)$ from the current data shown in Fig 1. With respect to the ΛCDM model as a base model, we plot the improvement of the χ^2 in panel (A) of Fig 2 and in Table I. We find that as N increases, the χ^2 generally decreases, showing an improvement of the fit with more w bins which is expected. Furthermore, the slope of $\Delta\chi^2$ varies with N, namely, when N goes from 3 to 5, the χ^2 drops quickly whereas $N < 3$ or $N > 5$, the χ^2 decreases slightly. As N increases from 1 to 3, $w(z)$ starts to deviate from -1. But this makes the χ^2 get only slightly improved, meaning that these binnings are too coarse to capture the features properly. When N grows to 4, a new pattern appears, say, all the w bins show deviations from -1 at 68% confidence level, and interestingly, the odd bin values become greater than -1 whereas the even bins drop below the -1 boundary. Compared to the case of $N = 3$, the resolution of $N = 4$ allows us to see a new feature, say, $w(z) < -1$ ($z \in [0.33, 0.66]$). This new feature might explain the 'drop' on the $\Delta\chi^2$ plot. As N reaches 5, the pattern of $w(z)$ resembles that of $N = 4$, namely,

$$w(z) > -1, \quad z \in \mathcal{S} = [0, 0.2] \cup [0.4, 1.0];$$
$$w(z) < -1, \quad z \in \bar{\mathcal{S}}. \tag{14}$$

but the dynamics is seemingly more pronounced – the deviations from -1 of the first three bins are enhanced to about 95% confidence level. This makes the $\Delta\chi^2$ take a nosedive again. When N exceeds 5, the $w(z)$ pattern

---

[6] In the limit of infinitely many SNe on the hubble diagram, the $\Delta\chi^2$ is independent of the binning if the underlying physical model of dark energy is cosmological constant.

TABLE I: The χ^2, $\chi^2_{\rm red}$ (reduced χ^2) and AIC, BIC values for various models. For each quantity, the difference with respect to the base model ΛCDM is also listed.

Model	χ^2	$\Delta\chi^2$	$\chi^2_{\rm red}(\times 10^3)$	$\Delta\chi^2_{\rm red}(\times 10^3)$	BIC	ΔBIC	AIC	ΔAIC
ΛCDM	3149.1	0	1057.0	0	3197.1	0	3161.1	0
$N = 1$	3147.8	-1.3	1056.9	-0.1	3203.9	6.8	3161.9	0.8
$N = 2$	3146.8	-2.3	1056.9	-0.1	3210.8	13.7	3162.8	1.7
$N = 3$	3146.2	-2.9	1056.9	-0.1	3218.2	21.1	3164.2	3.1
$N = 4$	3143.3	-5.8	1056.5	-0.5	3223.3	26.2	3163.3	2.2
$N = 5$	3139.7	-9.4	1055.6	-1.4	3227.7	30.6	3161.7	0.6
$N = 6$	3139.5	-9.6	1056.0	-1.0	3235.6	38.4	3163.5	2.4
$N = 7$	3139.4	-9.7	1056.3	-0.7	3243.4	46.3	3165.4	4.3
$N = 8$	3139.3	-9.8	1056.6	-0.4	3251.3	54.2	3167.3	6.2
$N = 9$	3139.2	-9.9	1056.9	-0.1	3259.3	62.2	3169.2	8.1
$N = 10$	3139.2	-9.9	1057.6	0.6	3267.2	70.1	3171.2	10.1
$\{w_0, w_a\}$	3146.7	-2.4	1056.9	-0.1	3210.7	13.6	3162.7	1.6

TABLE II: The mean values of the dark energy parameters with 68% and 95% C.L. error bars for $N = 5$ model and for the CPL model. For the $N = 5$ model, the constraints on the rotated parameters q's are also listed.

w_1	$-0.79^{+0.12+0.23}_{-0.12-0.24}$	q_1	$-0.93^{+0.07+0.13}_{-0.07-0.15}$
w_2	$-2.1^{+0.49+0.93}_{-0.51-0.79}$	q_2	$-1.2^{+0.14+0.26}_{-0.14-0.24}$
w_3	$0.89^{+1.1+1.8}_{-1.0-2.1}$	q_3	$-0.46^{+0.28+0.50}_{-0.28-0.57}$
w_4	$0.41^{+1.9+2.6}_{-1.8-3.0}$	q_4	$-0.38^{+0.55+0.83}_{-0.58-1.0}$
w_5	$-1.5^{+0.88+1.3}_{-0.91-1.4}$	q_5	$-1.1^{+0.37+0.62}_{-0.34-0.46}$
w_0	$-0.90^{+0.11+0.23}_{-0.11-0.22}$	w_a	$-0.24^{+0.56+0.98}_{-0.55-1.2}$

remains, but the χ^2 gets improved only marginally since all the main features have already been identified by 5 bins and there is little work left for the extra bins to do. This is in consistency with our foregoing 'intuitive guess' for the case of dark energy with dynamics.

To quantify the GoF for different N, we need to view the reduced χ^2 versus the number of w bins N shown in panel (B) of Fig 2 and in Table I. As we see, the improved $\chi^2_{\rm red}$ reaches its extremum at $N = 5$. This means that using five bins is sufficient to find all the important features on $w(z)$, and any extra bins are redundant. They dilute the constraints by introducing degeneracies, but can do little to improve the fit. Therefore $N = 5$ is the optimal number of bins we need.

Note, however, different model selection criteria may prefer different models. Here we consider two other widely used alternatives, the *Akaike information criterion* (AIC) [49] and the *Bayesian Information Criterion* (BIC) [50]. They both serve as tools to compare different models using a likelihood method, yet they base on different statistical arguments. For example, AIC stems from the minimization prescription of the Kullback-Leibler information entropy, yet BIC roots in the approximation
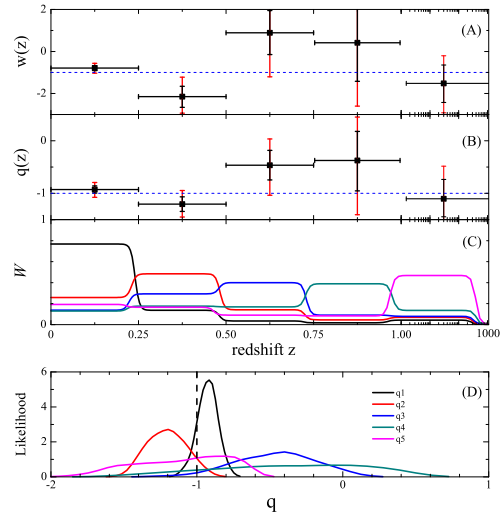

FIG. 4: Panel (A,B): The reconstructed $w(z)$ and $q(z)$ using 5 bins from current data. The vertical black and red error bars show 1σ and 2σ errors respectively. The blue dashed line shows ΛCDM model; Panel (C): The re-scaled window function $\mathcal{W}$; Panel (D): 1-D probability distribution of the q's.

of the Bayes factor. The AIC and BIC are defined as,

$$\text{AIC} = -2 \ln \mathcal{L} + 2 N_{\rm P} \qquad (15)$$

$$\text{BIC} = -2 \ln \mathcal{L} + N_{\rm P} \ln N_{\rm D} \qquad (16)$$

where $\mathcal{L}$ is the maximum likelihood, and $N_{\rm P}$ and $N_{\rm D}$ are the numbers of free parameters and that of the data points used in the fit, respectively. Viable models are supposed to minimize the quantities of AIC or BIC. The AIC

and BIC for different models are listed in Table I, which reads,

1. Both AIC and BIC favor the ΛCDM model;

2. Model of $N = 5$ is favored by the reduced χ^2 criterion, and is mildly disfavored by AIC;

3. All models except ΛCDM are strongly disfavored by BIC.

It is not surprising that AIC and BIC resist dynamical dark energy models because both AIC and BIC include strong penalty terms inhabiting the overfit – reducing χ^2 by introducing redundant free parameters. And if the number of data points exceeds $e^2 \sim 7$, which is often the case in cosmology, the penalty of BIC for additional parameters is stronger than that of the AIC. To be explicit, let's suppose one model has $\Delta N_{\rm P}$ additional free parameters compared to ΛCDM. If these $\Delta N_{\rm P}$ extra parameters can help reduce χ^2 by $2\Delta N_{\rm P}$, then it is preferred to ΛCDM by AIC. However, to satisfy BIC, the χ^2 must be reduced by three times more, i.e. $\Delta \chi^2 \sim 8\Delta N_{\rm P}$.

However, no matter favored or not by AIC or BIC, the dynamical dark energy model for the $N = 5$ case is worth investigating in depth since it reduces the χ^2 most for each degree of freedom, and the reconstructed $w(z)$ shows an excellent convergence. But unfortunately, this reconstruction is blurred by the correlations among all the w bins, making Fig 1 and Eq. (14) hard to interpret. The correlation between bins w_i and w_j is defined as,

$$ \mathrm{Corr}(w_i, w_j) = \frac{\mathrm{Cov}(w_i, w_j)}{\sigma(w_i)\sigma(w_j)}. \qquad (17) $$

where $\mathrm{Cov}(w_i, w_j)$ is the covariance between bins w_i and w_j, and $\sigma(w_i)$ and $\sigma(w_j)$ are standard deviations of w_i and w_j respectively. In Fig 3, we plot the correlation matrices for the cases of $N = 2$ to $N = 10$. As we can see, for the w bins centering at $z \lesssim 0.5$, there exists strong correlation between the neighboring bins. The last bin ($z \in [1, 1000]$) has little correlation with other bins, which explains why the constraint on this bin doesn't get diluted even if we have large number of redundant bins, as shown in Fig 1.

To de-correlate the bins, we apply the LPCA procedure explained in Sec. II to rotate the w's into q's, and we find,

$$ q(z) \begin{cases} > -1 \ (68\% \ C.L.), \ z \in [0, 0.25); \\ < -1 \ (\sim 95\% \ C.L.), \ z \in [0.25, 0.5); \\ > -1 \ (\sim 95\% \ C.L.), \ z \in [0.5, 0.75); \\ > -1 \ (68\% \ C.L.), \ z \in [0.75, 1); \\ \in [-1.44, -0.73] \ (68\% \ C.L.), \ z \geq 1. \end{cases} \qquad (18) $$

So at low redshift $z < 0.25$ or at high redshift $z \geq 0.75$, $q(z)$ is consistent with the ΛCDM prediction at the 95% confidence level. However, in the redshift range $[0.25, 0.75)$, $q(z)$ crosses the cosmological constant boundary,

and the error bars on the q's are uncorrelated thus free of degeneracy by design.

The detailed result of the LPCA is summarized in Table II and in Fig 4. From Panel (C) in Fig 4, we see that the window functions are almost positive and fairly localized, making the q's directly relate to the w's. This means that the q's have almost one-to-one correspondence with the original w bins. Therefore we can come to conclusion that the ΛCDM model is generally consistent with current data, yet Eq. (18) implies some hint, very weak though, on the possible dynamics of dark energy. In particular, a model predicting $w(z) < -1$ if $z \in [0.25, 0.5)$ and $w(z) > -1$ if $z \in [0.5, 0.75)$, which means that $w(z)$ crosses -1 in the range of $z \in [0.25, 0.75)$, is mildly favored.

Based on the best fit $w(z)$ from current data as the fiducial model, we can make the future forecast from JDEM, in combination of the Planck and LSST surveys. The results are shown in Fig 5. As we can see, the window functions are localized as that for the current data, and the error bars on $w(z)$ get shrink by roughly a factor of 8 and 13, for the cases with systematics and without systematics, respectively. Note that including systematics changes the correlations among the dark energy bins, which gives rise to the corresponding changes in $\mathcal{W}$ and the q's. Given the constraints on the q's, we can conclude that, if the fiducial model we derived from current data were true, then even for the most conservative case where the full systematics are included, JDEM combined with Planck and LSST would be able to detect a roughly 10σ deviation of $w(z)$ from -1.

It is useful to study the dependence of the results on the form of dark energy parametrizations. For an illustration, we compare the result we obtained so far to that from parametrization $\mathcal{X}_{\rm II}$, i.e., the CPL parametrization, and the result is summarized in Table I and in Fig 6. As shown, we find that the constraints on the CPL parameters from current data are

$$ w_0 = -0.90^{+0.11+0.23}_{-0.11-0.22}, \ w_a = -0.24^{+0.56+0.98}_{-0.55-1.2}. \qquad (19) $$

The central values indicate that the 'quintom B' scenario is mildly favored, namely, the EoS today $w(z)|_{z=0} = w_0 > -1$, while EoS in the far past $w(z)|_{z=\infty} = w_0 + w_a < -1$. This is consistent with the recent published result using the 'Constitution' SNe sample [51]. The contour plots of w_0 and w_a are shown as shaded grey regions in the right panel of Fig 6. We can see the best fit model from current data lies within the 'quintom B' region, and the ΛCDM model is consistent with current data at 1σ. Based on the current best fit model, future surveys has the ability to exclude ΛCDM model at 2σ and 5σ for the cases with and without the systematics respectively. In the left panels, we make a direct comparison of the reconstructed $w(z)$ from two different parametrizations – binned w and the CPL, shown in error bars and shaded regions respectively. Interestingly, we find that the $N = 2$ result agrees well with CPL (and the χ^2 for these two fits are very similar, see Table I), whereas for the case
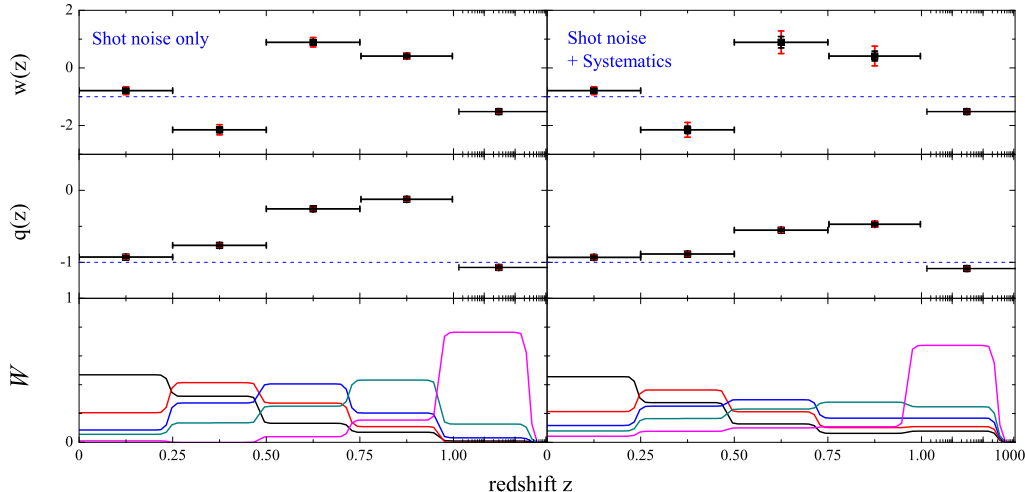
FIG. 5: Future forecasts from JDEM+Planck+LSST on $w(z), q(z)$ and the window functions. Left panels: Forecasts including statistical errors only; Right: Statistical plus systematic errors. The legends are the same as that for panels (A-C) in Fig 4.
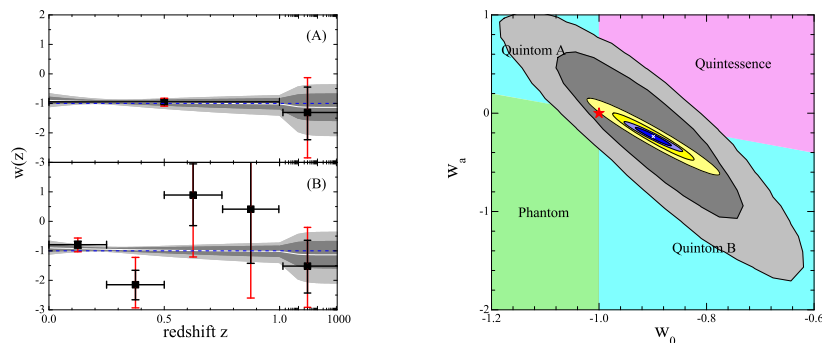

FIG. 6: Left: Comparison of the reconstructed $w(z)$ using two different parametrizations. The 68%(black) and 95%(red) C.L. error bars show the reconstructed $w(z)$ using parametrization $\mathcal{X}_{\mathrm{I}}$; The shaded regions show the $w(z)$ reconstruction using parametrization $\mathcal{X}_{\mathrm{II}}$. The inner and outer shades illustrate the 68% and 95% C.L. errors respectively, and central white line show the best fit model; Right: Contour plots for w_0, w_a. Grey: current data; Yellow: forecast from JDEM+Planck+LSST with systematics; Blue: forecast without systematics. For the same color, the dark and light shaded regions denote the 68% and 95% C.L. contours respectively. The red star stands for the ΛCDM model, and the white cross illustrates the current best fit model.

of $N = 5$, there is an apparent discrepancy. This is as expected – the results converge if the numbers of free parameters in the fit are the same, however, the CPL parametrization does not have enough freedom to resolve the local details of $w(z)$, resulting in the failure to capture the 'dip' and 'bump' happening at $0.25 \lesssim z \lesssim 0.75$.

IV. DISCUSSION AND SUMMARY

In this work, we have investigated the constraints on the general form of the equation-of-state of dark energy from the latest SNe, CMB and LSS data. We utilize a model-independent strategy – redshift binning plus PCA

– to extract information from data as much as possible. Starting from the most general parametrization – the w binning using the smooth tanh bins, we constrain the w bins using a MCMC algorithm while paying particular attention to the consistent implementation of the dark energy perturbations. We repeat this procedure for different binning scheme and investigate the goodness of fits using three different model selecting criteria – the reduced χ^2, AIC and BIC. While AIC and BIC strongly favor the ΛCDM model, the 5-w-bin model gives the maximum reduced χ^2, and we find a convergent evolution trend of $w(z)$ when $N \geq 4$.

We choose the model of $N = 5$ and rotate the w bins into the q bins to eradicate the correlations using a LPCA

method, and we found that at low redshift $z < 0.25$ or at high redshift $z \geq 0.75$, $q(z)$ is consistent with -1 at the 95% confidence level. However, in the intermediate redshift range [0.25, 0.75], $q(z)$ crosses the cosmological constant boundary. Since the q's have almost one-to-one correspondence with the original w bins by design, we can draw the conclusion that the ΛCDM model is generally consistent with the current data, yet there exists some weak hint of the possible dynamics of dark energy. In particular, a quintom model predicting $w(z) < -1$ if $z \in [0.25, 0.5)$ and $w(z) > -1$ if $z \in [0.5, 0.75)$, which means that $w(z)$ crosses -1 in the range of $z \in [0.25, 0.75)$, is mildly favored.

Note that the measurement of the luminosity distance is crucial to study dark energy dynamics, thus our results are sensitive to the choice of the SN data set and analysis. The apparent dynamics of dark energy we found using the published 'Constitution' SNe sample might be physical, but there is another possibility of the artifacts in the SNe data analysis. Therefore we have planned a careful study of the effect of SN sample on dark energy constraints.

Given the best fit model from current data, we make a forecast from the upcoming/future surveys of JDEM, Planck and LSST, and we find that the future data are able to shrink the error bars on the dark energy bins by roughly a factor of 10, which is promising to find the smoking gun of the dark energy evolution.

Note added: After completion of this work, we noticed another analysis on $w(z)$ using different dataset and method [22]. Although both our work and Ref. [22] claim that the cosmological constant is favored at 95% CL., Ref. [22] found less preference of dark energy dynamics. This difference may stem from the difference in data selection and analyzing prescription, and it is worth further investigating.

[1] A. G. Riess *et al.*, Astron. J. **116**, 1009 (1998).

[2] S. Perlmutter *et al.*, Astrophys. J. **517**, 565 (1999).

[3] A. A. Starobinsky, Phys. Lett. B **91**, 99 (1980).

[4] S. Capozziello, S. Carloni and A. Troisi, Recent Res. Dev. Astron. Astrophys. **1**, 625 (2003).

[5] S. M. Carroll, V. Duvvuri, M. Trodden and M. S. Turner, Phys. Rev. D **70**, 043528 (2004).

[6] A. A. Starobinsky, JETP Lett. **86**, 157 (2007).

[7] S. Nojiri and S. D. Odintsov, arXiv:0801.4843 [astro-ph].

[8] B. Boisseau, G. Esposito-Farese, D. Polarski and A. A. Starobinsky, Phys. Rev. Lett. **85**, 2236 (2000).

[9] J. Khoury and A. Weltman, Phys. Rev. Lett. **93**, 171104 (2004).

[10] G. R. Dvali, G. Gabadadze and M. Porrati, Phys. Lett. B **485**, 208 (2000).

[11] G. Dvali, S. Hofmann and J. Khoury, Phys. Rev. D **76**, 084006 (2007).

[12] B. Ratra and P. J. E. Peebles, Phys. Rev. D **37**, 3406 (1988).

[13] R. R. Caldwell, Phys. Lett. B **545**, 23 (2002).

[14] B. Feng, X. L. Wang and X. M. Zhang, Phys. Lett. B **607**, 35 (2005).

[15] U. Seljak *et al.* [SDSS Collaboration], Phys. Rev. D **71**, 103515 (2005); A. Upadhye, M. Ishak and P. J. Steinhardt, Phys. Rev. D **72**, 063501 (2005); S. Hannestad and E. Mortsell, JCAP **0409**, 001 (2004); P. S. Corasaniti, M. Kunz, D. Parkinson, E. J. Copeland and B. A. Bassett, Phys. Rev. D **70**, 083006 (2004); V. Sahni and A. Starobinsky, Int. J. Mod. Phys. D **15**, 2105 (2006); J. Q. Xia, G. B. Zhao, B. Feng, H. Li and X. Zhang, Phys. Rev. D **73**, 063521 (2006); D. F. Mota, J. R. Kristiansen, T. Koivisto and N. E. Groeneboom, Mon. Not. Roy. Astron. Soc. **382**, 793 (2007); G. B. Zhao, J. Q. Xia, B. Feng and X. Zhang, Int. J. Mod. Phys. D **16**, 1229 (2007); G. B. Zhao, J. Q. Xia, H. Li, C. Tao, J. M. Virey, Z. H. Zhu and X. Zhang, Phys. Lett. B **648**, 8 (2007); J. Q. Xia, H. Li, G. B. Zhao and X. Zhang, Phys. Rev. D **78**, 083524 (2008); J. Q. Xia, M. Viel, C. Baccigalupi and S. Matarrese, arXiv:0907.4753 [astro-ph.CO]; J. Q. Xia and M. Viel, JCAP **0904**, 002 (2009).

[16] M. Chevallier and D. Polarski, Int. J. Mod. Phys. D **10**, 213 (2001).

[17] E. V. Linder, Phys. Rev. Lett. **90**, 091301 (2003).

[18] B. Feng, M. Li, Y. S. Piao and X. Zhang, Phys. Lett. B **634**, 101 (2006); J. Q. Xia, B. Feng and X. M. Zhang, Mod. Phys. Lett. A **20**, 2409 (2005); E. V. Linder, Astropart. Phys. **25**, 167 (2006); J. Liu, H. Li, J. Xia and X. Zhang, JCAP **0907**, 017 (2009).

[19] J. Q. Xia, G. B. Zhao, H. Li, B. Feng and X. Zhang, Phys. Rev. D **74**, 083521 (2006).

[20] D. Huterer and G. Starkman, Phys. Rev. Lett. **90**, 031301 (2003).

[21] G. B. Zhao, D. Huterer and X. Zhang, Phys. Rev. D **77**, 121302 (2008).

[22] P. Serra, A. Cooray, D. E. Holz, A. Melchiorri, S. Pandolfi and D. Sarkar, arXiv:0908.3186 [astro-ph.CO].

[23] W. Hu, Phys. Rev. D **66**, 083515 (2002).

[24] R. G. Crittenden and L. Pogosian, arXiv:astro-ph/0510293.

[25] R. de Putter and E. V. Linder, Astropart. Phys. **29**, 424

(2008).

[26] R. de Putter and E. V. Linder, arXiv:0812.1794 [astro-ph].

[27] G. B. Zhao, L. Pogosian, A. Silvestri and J. Zylberberg, arXiv:0905.1326 [astro-ph.CO].

[28] D. Huterer and A. Cooray, Phys. Rev. D **71**, 023506 (2005).

[29] C. Stephan-Otto, Phys. Rev. D **74**, 023507 (2006).

[30] A. Shafieloo, U. Alam, V. Sahni and A. A. Starobinsky, Mon. Not. Roy. Astron. Soc. **366**, 1081 (2006) [arXiv:astro-ph/0505329].

[31] Y. Wang and P. Mukherjee, Phys. Rev. D **76**, 103533 (2007); Y. Wang, arXiv:0910.2492 [astro-ph.CO].

[32] J. Weller and A. M. Lewis, Mon. Not. Roy. Astron. Soc. **346**, 987 (2003).

[33] G. B. Zhao, J. Q. Xia, M. Li, B. Feng and X. Zhang, Phys. Rev. D **72**, 123515 (2005).

[34] W. Fang, W. Hu and A. Lewis, Phys. Rev. D **78**, 087303 (2008).

[35] http://jdem.gsfc.nasa.gov/

[36] A. Lewis and S. Bridle, Phys. Rev. D **66** 103511 (2002).

[37] M. Hicken *et al.*, arXiv:0901.4804 [astro-ph.CO].

[38] E. Komatsu, *et al.*, arXiv: 0803.0547; J. Dunkley, *et al.*, arXiv: 0803.0586; E. L. Wright, *et al.*, arXiv: 0803.0577; M. R. Nolta, *et al.*, arXiv: 0803.0593; B. Gold, *et al.*, arXiv: 0803.0715; G. Hinshaw, *et al.*, arXiv: 0803.0732.

[39] M. Tegmark *et al.*, Phys. Rev. D **74** 123507 (2006).

[40] W. L. Freedman, *et al.*, Astrophys. J. **553**, 47 (2001).

[41] S. Burles, K. M. Nollett and M. S. Turner, Astrophys. J. **552**, L1 (2001).

[42] http://www.rssd.esa.int/index.php?project=planck

[43] http://www.lsst.org/

[44] G. B. Zhao, L. Pogosian, A. Silvestri and J. Zylberberg, Phys. Rev. D **79**, 083513 (2009).

[45] M. Tegmark, A. Taylor and A. Heavens, Astrophys. J. **480**, 22 (1997).

[46] W. Hu and B. Jain, Phys. Rev. D **70**, 043009 (2004).

[47] D. Huterer, M. Takada, G. Bernstein and B. Jain, Mon. Not. Roy. Astron. Soc. **366**, 101 (2006); H. Zhan, L. Knox and J. A. Tyson, Astrophys. J. **690**, 923 (2009).

[48] A. R. Zentner, D. H. Rudd and W. Hu, Phys. Rev. D **77**, 043507 (2008).

[49] H. Akaike, 1974, IEEE Trans. Auto. Control, 19, 716

[50] G. Schwarz, 1978, Annals of Statistics, 5, 461

[51] A. Shafieloo, V. Sahni and A. A. Starobinsky, arXiv:0903.5141 [astro-ph.CO]; R. 1. Biswas and B. D. Wandelt, arXiv:0903.2532 [astro-ph.CO]; S. Qi, T. Lu and F. Y. Wang, arXiv:0904.2832 [astro-ph.CO]; H. Wei, arXiv:0906.0828 [astro-ph.CO]; Q. G. Huang, M. Li, X. D. Li and S. Wang, Phys. Rev. D **80**, 083515 (2009).